PROCEEDINGS, 47th Workshop on Geothermal Reservoir Engineering
Stanford University, Stanford, California, February 7-9, 2022
SGP-TR-223

Spatial-Temporal Stress Heterogeneity in the Geothermal Reservoir at San Emidio, Nevada, U.S.

Benjamin J. JAHNKE (1), Hao GUO (1), Ben HEATH (1), Erin CUNNINGHAM (1), Chris SHERMAN (2), Hiroki SONE (1), Ian WARREN (3), Corné KREEMER (4), Clifford H. THURBER (1), Kurt L. FEIGL (1), and the WHOLESCALE Team

(1) University of Wisconsin-Madison, Department of Geoscience, Madison, WI, United States
(2) Lawrence Livermore National Laboratory, Livermore, CA, United States
(3) National Renewable Energy Lab (NREL), Golden, CO, United States
(4) University of Nevada, Reno, NV, United States

bjahnke3@wisc.edu

Keywords: WHOLESCALE, San Emidio, EGS, Stress, Stress Inversion

ABSTRACT

We attempt to constrain models of the reservoir stress of a geothermal reservoir in San Emidio, Nevada, which will be used in a reservoir-scale hydro-mechanical numerical model. Our reservoir stress models are based on (1) the densities of subsurface lithologies, (2) surface topography, (3) the relative magnitudes of the total vertical stress (SV), maximum horizontal stress (SHmax), and minimum horizontal stress (Shmin), and (4) the azimuth of SHmax. The models are informed from stress indicators within a ~175 km radius of San Emidio which provides constraints on (1) the relative magnitudes of SV, SHmax, and Shmin, and (2) the azimuth of SHmax. To evaluate how well the model represents the reservoir stress, focal mechanism data from microseismic events which occurred within the reservoir during a plant shutdown in 2016 are used. Stress inversions (Vavryčuk, 2014) of the focal mechanism data estimate the *in situ* principal stress orientations, their relative magnitudes, and preferred nodal planes. Then the principal orientations of the model stresses at the locations of microseismic events were compared to the principal stress orientations inverted from the focal mechanisms. These analyses allow us to refine the reservoir stress model that agrees with field observations and is therefore suitable to use to forward model the reservoir responses against production and injection operations. In this paper, we provide a snapshot of work in progress, including the highlights listed in the conclusions below. The work presented herein has been funded in part by the Office of Energy Efficiency and Renewable Energy (EERE), U.S. department of Energy, under Award Numbers DE-EE0007698 and DE-EE0009032.

1. INTRODUCTION

The aim of the WHOLESCALE project is to understand the *in situ* stress within the geothermal reservoir located at San Emidio, Nevada, United States. This is being done through comparison of a reservoir-scale GEOSX stress model and geophysical observations. The goal of the reservoir stress model is to simulate the stresses responsible for four types of observational data, including (1) microseismic event locations, (2) borehole breakouts and drilling induced tensile fractures observed in wellbores, (3) ground surface displacements, and (4) pore fluid pressures. In this study, focal mechanisms from microseismic events within the reservoir are used to estimate the orientations and relative magnitudes of principal stress.

In the late 1970s, early exploration of the San Emidio region began by several companies conducting surveys and drilling wells (Folsom et al., 2020). This early exploration defined a shallow geothermal reservoir, with temperatures reaching ~134 °C (Matlick, 1995). In the mid to late 1980s, the Empire power plant drilled more than a dozen wells targeting this shallow reservoir. In 1987, the AMOR II Corp commissioned a 3.6 MW binary power plant which used the shallow wells. In the early 1990s, Empire drilled deeper wells discovering a deeper reservoir. In 2008, U.S. Geothermal acquired the Empire power plant and began to maximize the wellfield. In 2012, a 14.7 MW power plant was commissioned. This resulted in the drilling of exploration wells which defined a deeper, hotter reservoir, with temperatures reaching 154 – 161 °C. In 2015, exploration wells were deepened such that three wells encountered commercial temperatures and permeability.

The geothermal operating plant at San Emidio is composed of a system of injection and production wells that circulate water throughout faults and fractures within the reservoir. Using daily pumping data, the cumulative produced and injected volumes at San Emidio from 1997-2020 are shown in Figure 1. Except during 2003-2004, the rate of net production is relatively low.

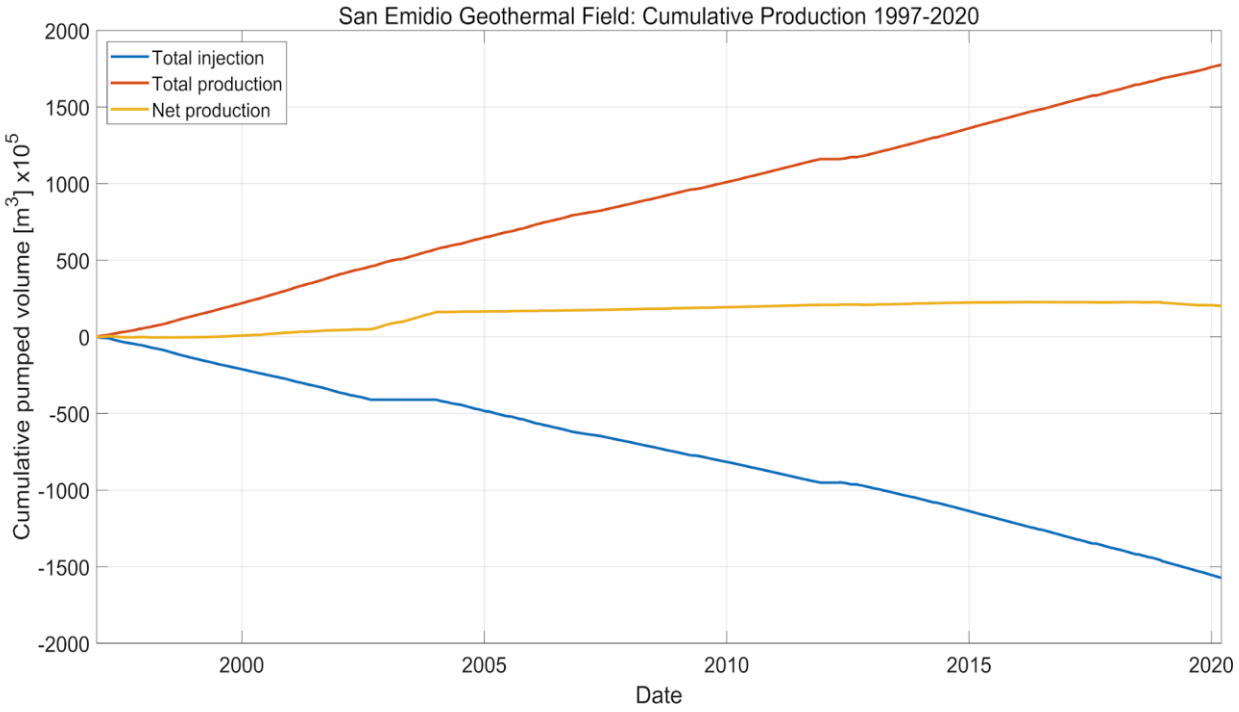

Figure 1: Cumulative pumped fluid volumes at the San Emidio geothermal field from 1997-2020. Red curve indicates total production volumes, blue curve indicates total injection volumes, and yellow curve indicates net production.

In December of 2016, all active injection and production wells were shut-in temporarily, stopping all fluid flow into and out of the reservoir for about one day. A total of 122 microseismic events were recorded from which focal mechanisms could be determined for 31 of the events. Using the events with focal mechanism solutions, stress inversions were performed to infer the reservoir stress state at the time of the shut-in. The results of the stress inversions determined from the focal mechanism solutions are then compared to the stress directions determined in the stress models at the locations of the microseismic events. The degree to which the inverted stress directions agree with the modeled stress directions indicates how well the stress model represents the reservoir stress state.

Spatial and temporal heterogeneities of reservoir stress throughout the duration of the shut-in are also investigated. To investigate the extent of spatial and temporal stress within the reservoir, the microseismic events were sorted into spatial and temporal clusters. Then, stress inversions (Vavryčuk, 2014) were performed using the focal mechanism data to infer the reservoir stress and distinguish between the auxiliary and slip planes, which provides fault orientations. Using the inverted stress states from the clustered focal mechanisms, the reservoir stress can be compared with both the background regional tectonic stress and stress models.

2. GEOLOGIC SETTING

The geothermal reservoir is located in the San Emidio desert of northwestern Nevada, United States. The reservoir itself is in a fractured rock volume with a network of westward dipping normal faults shown in Figure 2 (Folsom et al, 2020). The shallower and cooler parts of the reservoir are composed of poorly lithified sedimentary sequences, whereas the deeper and hotter parts of the reservoir are composed of low porosity volcanic and metamorphic rocks. Due to the low porosity in the deeper and hotter rocks, fluid transport is concentrated in faults and fractures.

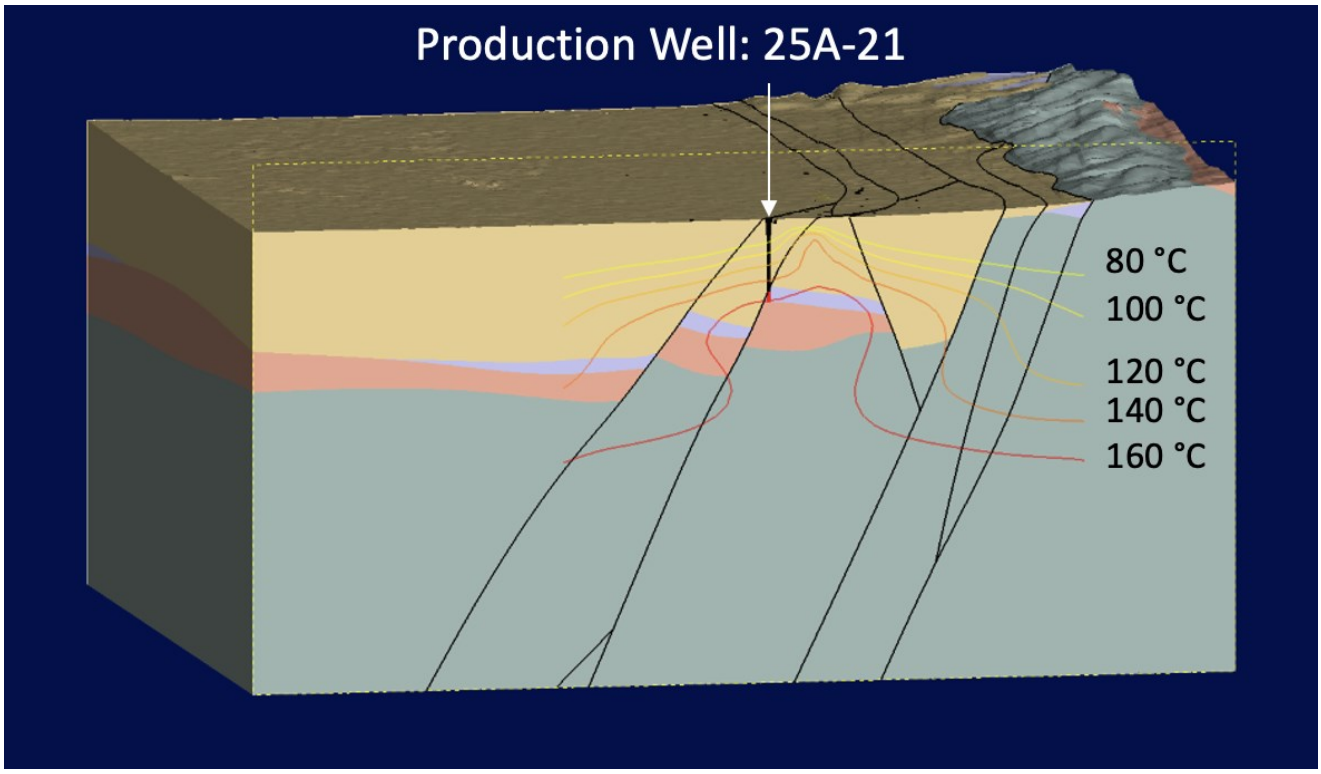

Figure 2: East-west cross-section of the subsurface geology at San Emidio. The cross-section shows the profile of production well 25A-21. The geothermal reservoir is within the series of westward dipping normal faults extending from the sedimentary rocks downwards into volcanic and metamorphic rocks. Isotherms have been contoured onto the cross-section. Figure from Folsom et al (2020).

A first-order estimation of the background regional tectonic stress is inferred using information from the World Stress Map (Heidbach et al., 2018) and wellbore indicators in the form of breakouts and drilling induced tensile fractures observed in nearby geothermal fields. Stress indicators within a ~175 km radius surrounding San Emidio are considered to be representative of the background regional tectonic stress (Figure 3). Stress indicators from the World Stress Map primarily come from earthquake focal mechanisms, which indicate an SHmax azimuth close to N10E and a normal or strike-slip stress regime. Wellbore indicators from nearby wells from Astor Pass (Siler et al., 2016), Dixie Valley (Hickman et al., 1998), and Desert Peak (Hickman & Davatzes, 2010) indicate SHmax azimuths of N3E ± 12°, N33E ± 10°, and N24E ± 17°, respectively. Additionally, the faulting regimes at Astor Pass, Dixie Valley, and Desert Peak are strike-slip, normal, and normal/strike-slip, respectively. Although not an indicator of stress, the direction of maximum contractional secular strain rate is N3E at San Emidio (Kreemer et al., 2014) indicating that the background regional tectonic stress and strain appear to be subparallel. Figure 4 summarizes the regional SHmax directions outlined above.

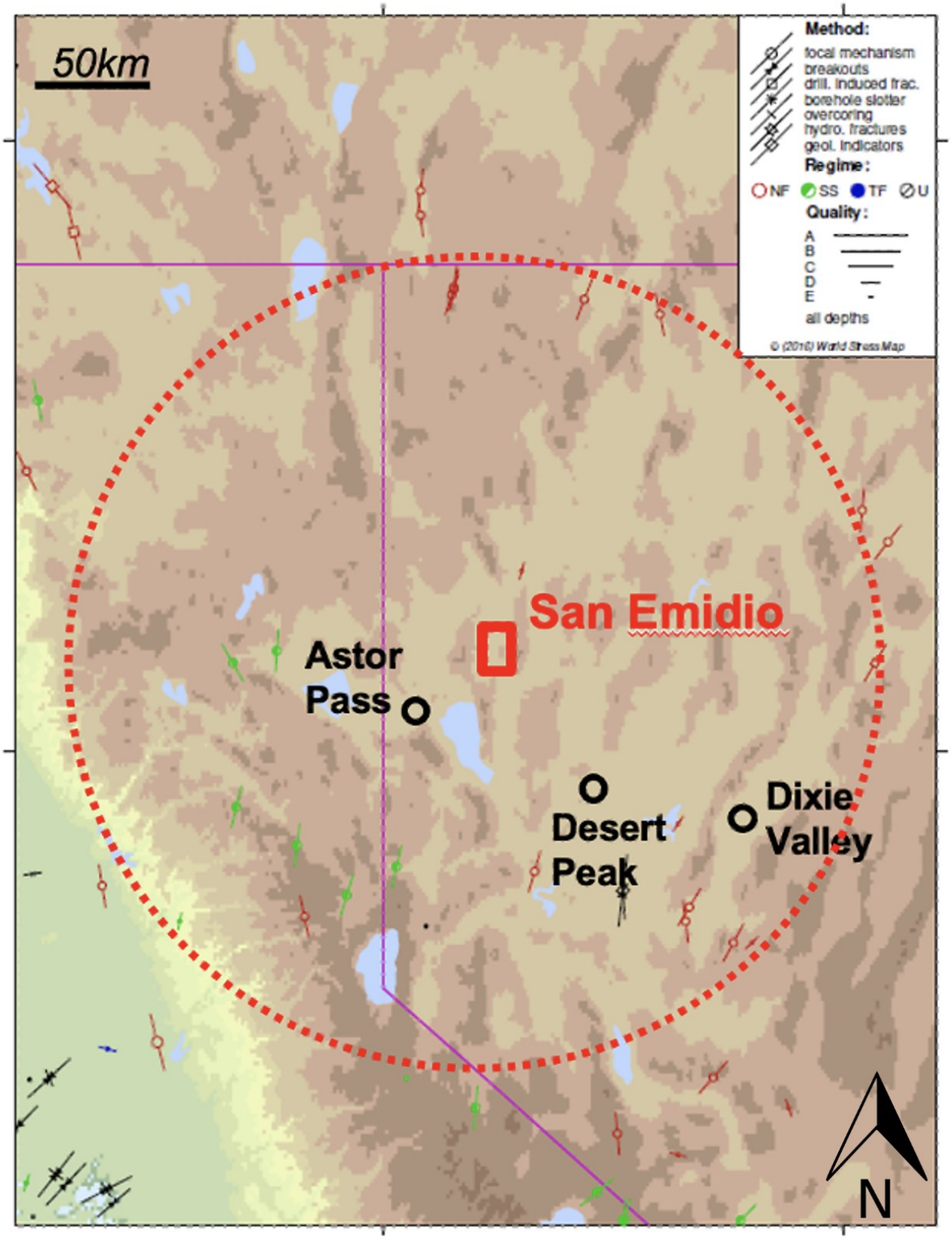

Figure 3: World Stress Map with locations of stress indicators within a ~175 km radius (red dashed circle) around San Emidio (red rectangle). Line segments with circles indicate locations of earthquake focal mechanisms. The orientation of the line segments delineates the $S_{H,\,max}$ azimuth, and the color indicates the stress regime (red = normal, green = strike-slip). Black circles indicate the locations of nearby wells with wellbore stress indicators, such as breakouts and drilling induced tensile fractures

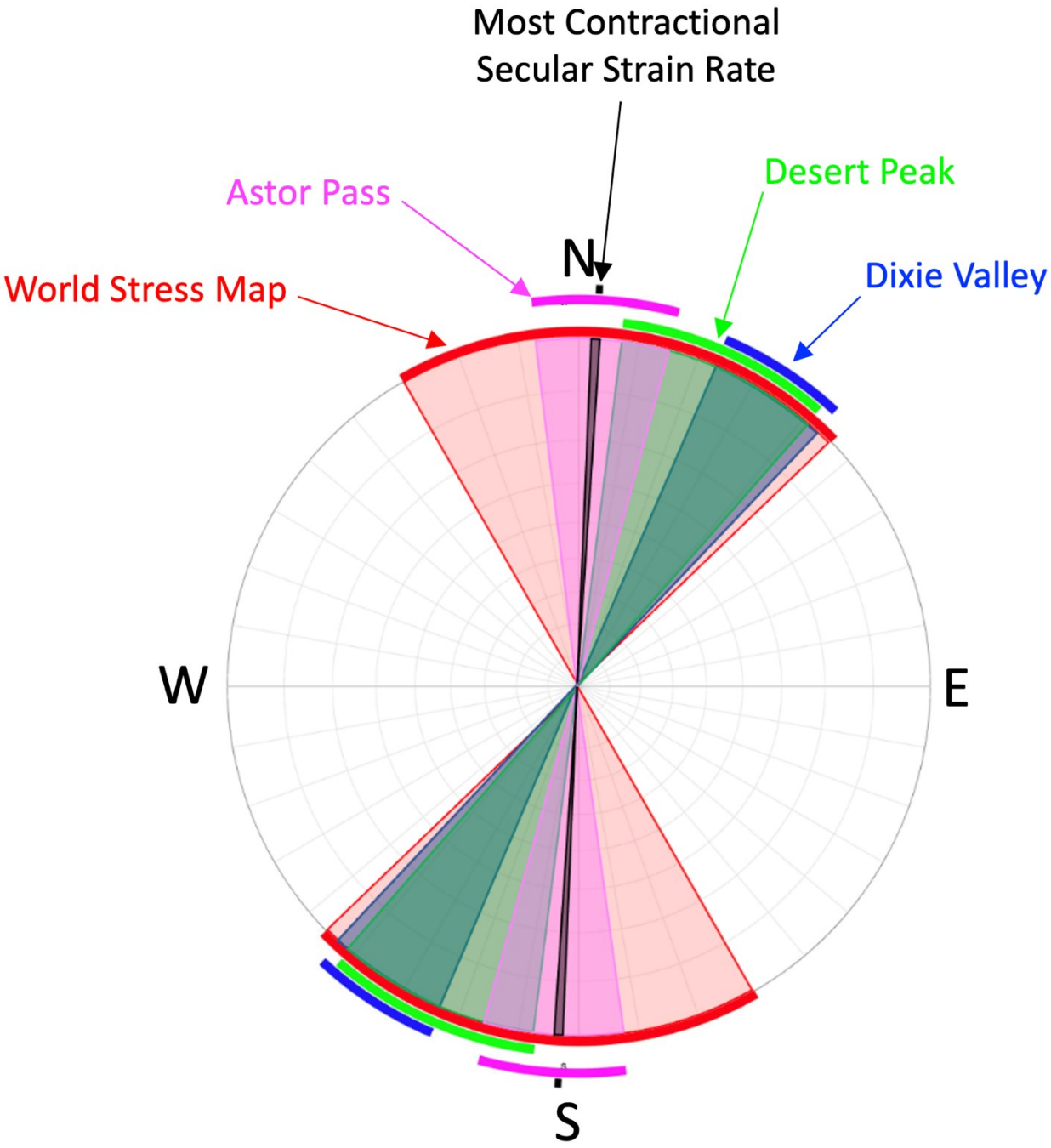

Figure 4: Summary of regional observations of SHmax azimuths. Red shaded regions indicate range of SHmax azimuths from observations documented in the World Stress Map (Heidbach et al., 2018). Green, blue, and pink shaded regions indicate ranges of SHmax azimuths from wellbore indicators from Desert Peak (Hickman & Davatzes, 2010), Dixie Valley (Hickman et al., 1998), and Astor Pass (Siler et al., 2016), respectively. Black shaded region indicates the direction of the most compressive secular strain azimuth, or direction of maximum contractional strain rate (Kreemer et al., 2014).

The GEOSX reservoir stress model is a 3-dimensional model that computes the 3D stress tensor within a meshed volume (Figure 5). Densities are to obtain a vertical stress profile throughout the model. Horizontal stress profiles are obtained assuming a hydrostatic pore pressure gradient, critically stressed conditions, a vertical principal stress, and an SHmax azimuth constrained by the summary of regional observations of SHmax. Then, gravity is turned on such that the model is equilibrated with topography by running an implicit solver.

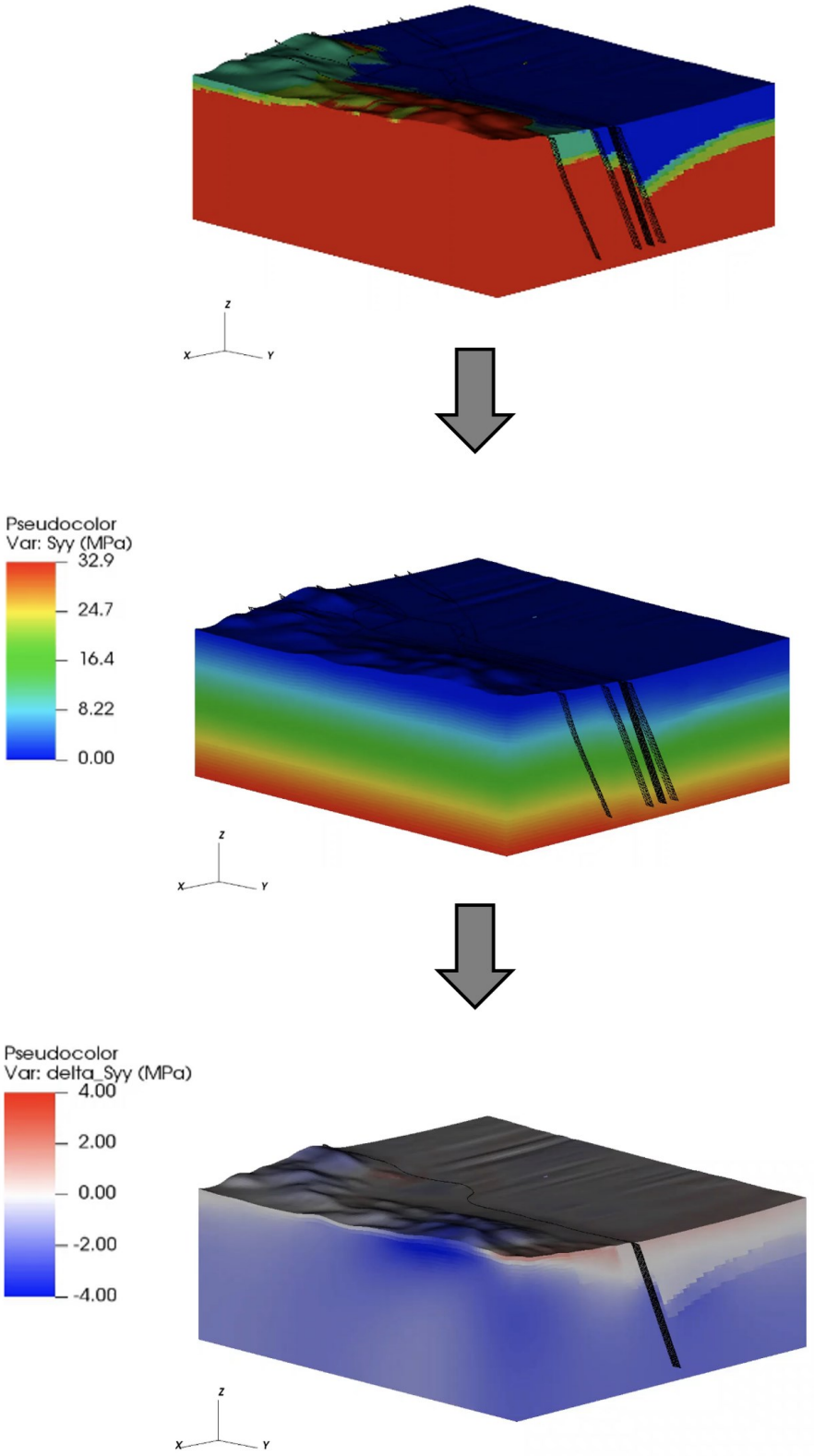

Figure 5: Schematic diagrams of how the GEOSX reservoir stress model is generated. It starts with (1) a density model used for (2) a depth-dependent calculation of vertical stress (maximum and minimum horizontal stress calculations are based on frictional strength limits). Then, (3) gravity is turned on, and the model is equilibrated with boundaries by running an implicit solver.

3. METHODS

To attempt to characterize the reservoir stress heterogeneity in space and time, the 31 focal mechanisms were clustered into spatial and temporal groups. Spatially clustered focal mechanisms were clustered based on hypocenter location, and sense of slip. Temporally clustered focal mechanisms were clustered based on their occurrence time throughout the duration of the shut-in. In total, five spatial clusters and three temporal clusters were formed, shown in Figure 7.

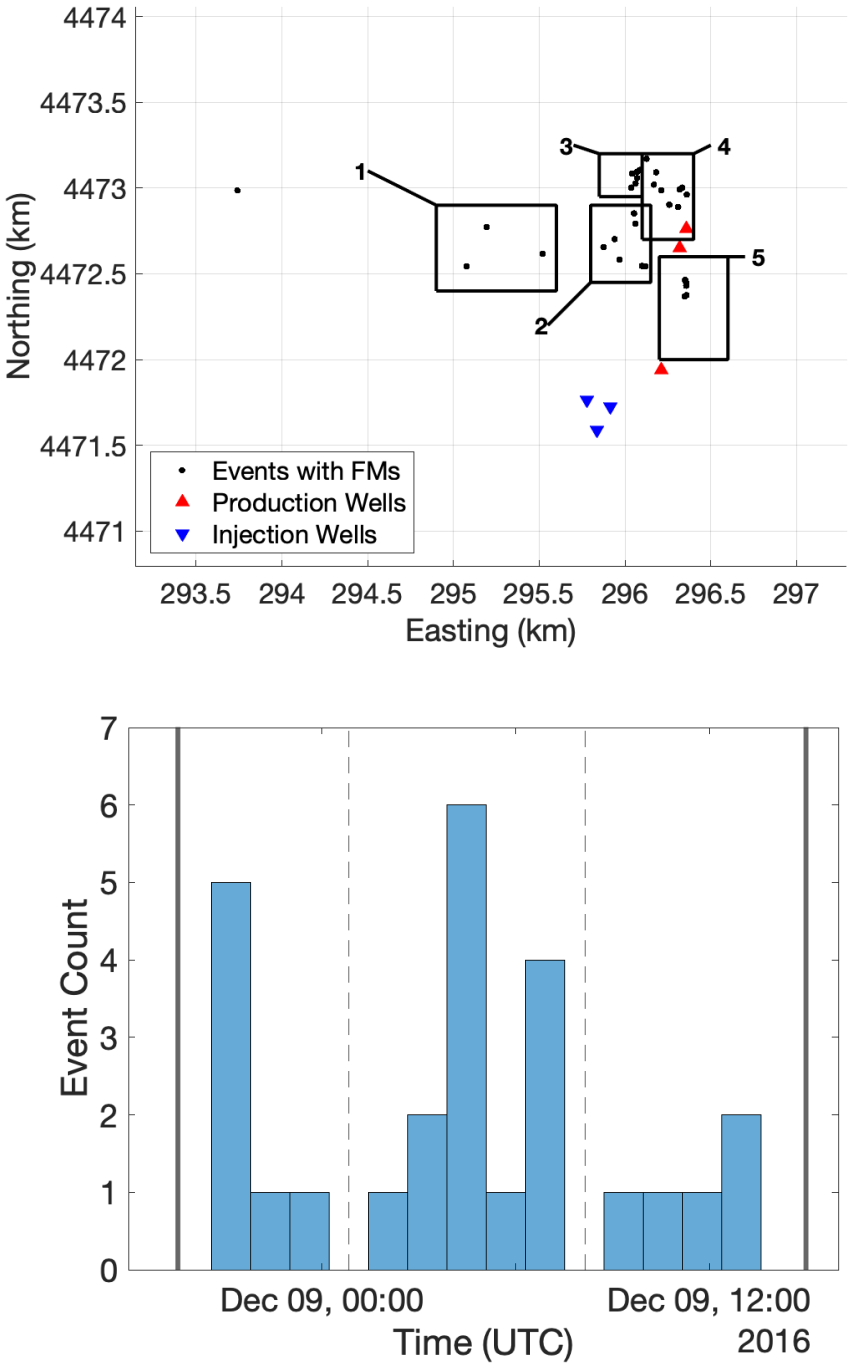

Figure 7: Spatial clusters (top) and temporal clusters (bottom) of microseismic events. (Top) Black circles indicate locations of microseismic events with focal mechanism solutions. Red and blue triangles indicate production and injection wells, respectively. (Bottom) Solid vertical lines indicate the start and stop times of the shut-in. Dashed vertical lines indicate boundaries between the three temporal groups.

Focal mechanism solutions obtained from the 2016 shut-in were used to perform linear stress inversions (Michael, 1984). Stress inversions use fault slip data to estimate a stress state that minimizes the difference between fault slip vectors and the direction of maximum shear

traction on each fault plane. Since focal mechanisms do not explicitly differentiate between the auxiliary and slip plane, an iterative joint inversion (Vavryčuk, 2014) was performed on the focal mechanism data to simultaneously identify the probable slip planes. To differentiate between the fault plane and auxiliary plane, the iterative joint inversion introduces the fault instability constraint. The fault instability constraint indicates how stable a given fault plane is given a stress state. Given an inverted stress state from a randomly selected set of nodal planes from each focal mechanism used in an inversion, the iterative joint inversion method determines the stability of both nodal planes for each focal mechanism solution (Figure 8). Then, given the inverted stress state, the nodal plane closest to failure for each focal mechanism can be used for subsequent stress inversions. This procedure of calculating fault instability and then selecting the more unstable nodal plane is iterated until a set of nodal planes is converged on.

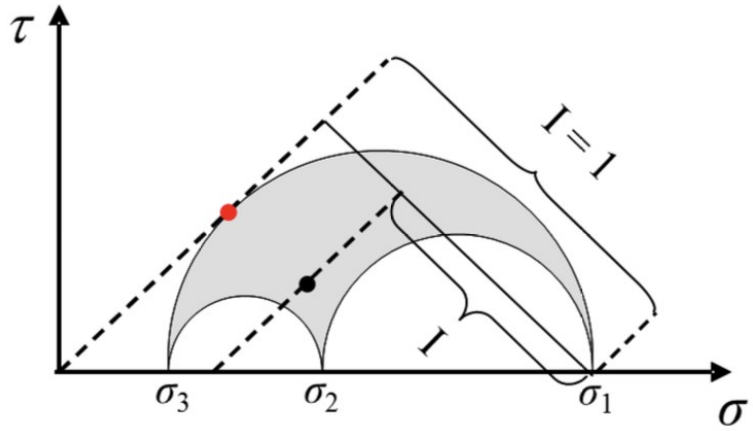

Figure 8: Fault stability represented in a Mohr diagram. The red dot indicates the normal and shear tractions on the optimally oriented fault plane with fault instability I = 1. The black dot indicates the normal and shear tractions on an arbitrarily oriented fault with instability I. Figure form Vavryčuk (2014).

In theory, the results of the iterative joint inversion should produce the slip planes providing fault slip orientation within the reservoir from focal mechanism solutions. However, the initial choice of nodal planes can influence the final converged inverted stress state. The final set of nodal planes determined to be most unstable can be dependent on the initial choice of nodal planes for each inversion. Therefore, it is possible for multiple stress states to be inverted from a set of focal mechanisms.

The average misfit angle is determined for each stress inversion. The misfit angle is the angle between the fault slip vectors and orientation of maximum shear traction defined by the inverted stress state on each fault plane. The misfit angle is a metric that describes how well the inverted stress state describes the fault data. A smaller misfit angle indicates an inverted stress state that fits the fault slip data well.

The shape ratio, R, is also determined for each stress inversion:

$$R = \frac{\sigma_1 - \sigma_2}{\sigma_1 - \sigma_3} \quad (1)$$

where σ_1, σ_2, and σ_3, are the normalized magnitudes of the principal stresses. Shape ratios range between 0 and 1. A shape ratio near 0 or 1 indicates a stress state two of the three principal stresses are close in magnitude.

4. RESULTS

The results of the stress inversions using all focal mechanisms from the 2016 shut-in are plotted on stereonets shown in Figure 9. The inverted stress state indicates a σ_1 near vertical, σ_2 near horizontal oriented North/South, and σ_3 near horizontal oriented East/West.

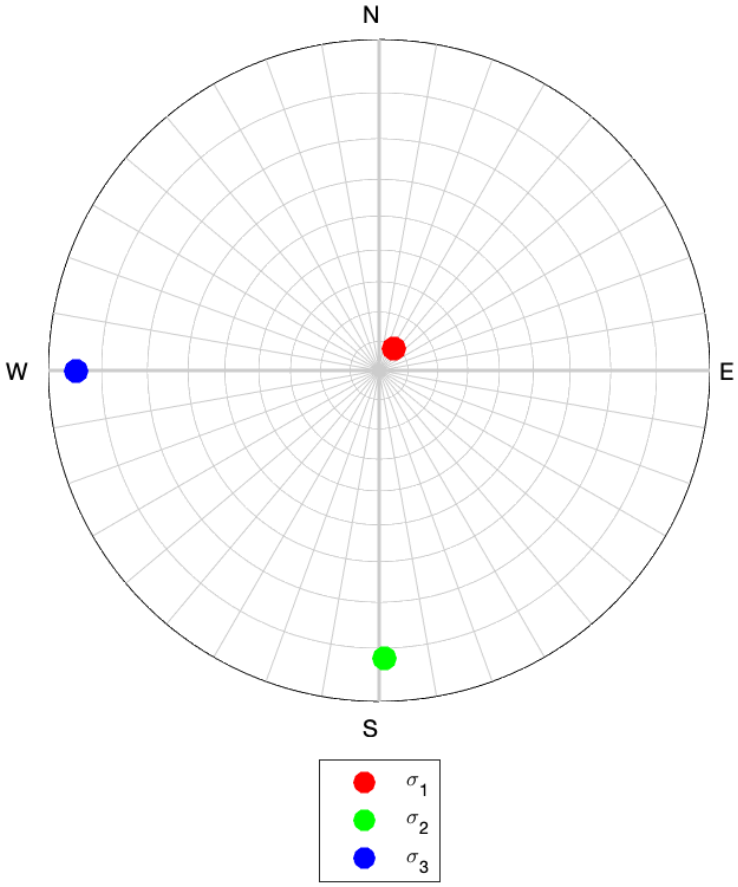

Figure 9: Stress inversion results using all focal mechanisms. The red, green, and blue markers correspond to the inverted directions of σ_1, σ_2, and σ_3, respectively.

The results of the stress inversions using the focal mechanisms for each of the spatial clusters are plotted on stereonets (Figure 10). Independent of the initial choices of nodal planes, clusters S1, S2, and S4 converged into a single inverted stress state. However, the inverted stress states of clusters S2 and S5 showed a dependence on the initial combination of nodal planes used in the iterative joint inversion. σ_1 is oriented near vertical for all spatial clusters except for S4 where σ_2 is the principal stress oriented nearest vertical. There is some variance of the inverted σ_2 orientation depending on the spatial cluster. Although the inverted σ_2 orientations of S1, S3, and S5 are not completely horizontal, their trends are within the range of observed regional SHmax azimuths. S2 contains one possible inverted stress state with σ_2 oriented near horizontal, with a trend consistent with the regional SHmax azimuth. However, in S2 there is one possible stress state with σ_2 oriented near horizontal with a trend at the margin of observed regional SHmax azimuths, and another possible inverted stress state with σ_2 oriented near horizontal, but with a trend completely inconsistent with observed regional SHmax azimuths. The shape ratios are relatively high for two of the three inverted stress states for S2, which may make it difficult to discern an SHmax azimuth from the data. The inconsistencies between the numerous converged stress states from S2, resulting from the difference in initial choices of the nodal planes, suggest that a single stress state cannot be inferred to explain the occurrence of events in S2.

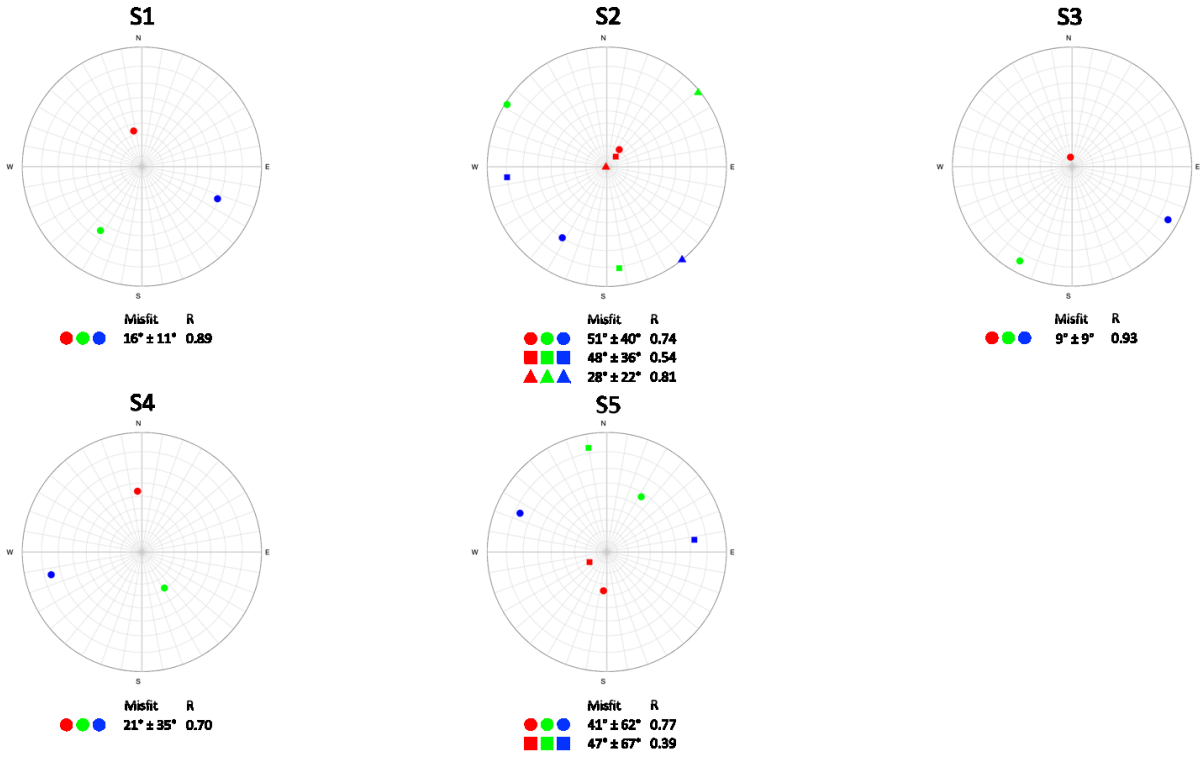

Figure 10: Stress inversion results for spatially clustered microseismic events. The red, green, and blue markers correspond to the inverted orientations of σ_1, σ_2, and σ_3, respectively. Markers of similar shape correspond to unique inverted stress states.

The results of the stress inversions using the focal mechanisms within the temporal clusters are plotted on stereonets shown in Figure 11. The inverted stress states of all spatial clusters showed a dependence on the initial combination of nodal planes used in the stress inversions. σ_1 is oriented near vertical for all temporal clusters. There is some variance of the inverted σ_2 orientation depending on the temporal cluster. The inverted σ_2 orientations of T1 are near horizontal, but with trends completely inconsistent with observed regional SHmax azimuths. However, the inverted σ_2 orientations of T1 are clustered in an East/West to Northwest/Southeast orientation. The inverted σ_3 orientations of T1 are more consistent with the regional SHmax azimuths. Although the inverted σ_2 orientations of T2 and T3 are not completely horizontal, their trends are within the range of observed regional SHmax azimuths.

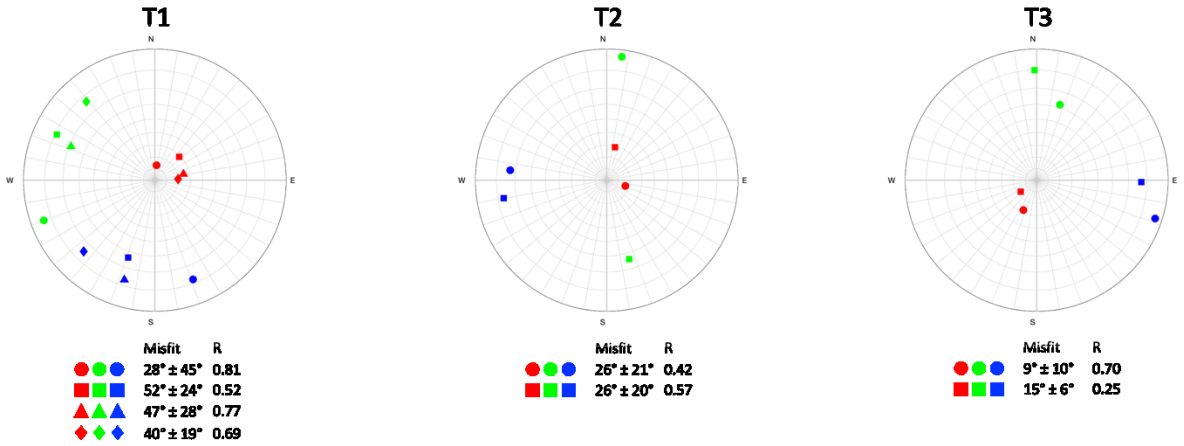

Figure 11: Stress inversion results for temporally clustered microseismic events. The red, green, and blue markers correspond to the inverted orientations of σ_1, σ_2, and σ_3, respectively. Markers of similar shape correspond to unique inverted stress states.

5. DISCUSSION

Depending on which focal mechanisms were used in the stress inversions, there appears to be a range of possible stress states within the reservoir. The stress inversion which used all events suggests a normal faulting environment, with a near vertical σ_1, and a near horizontal, North/South trending σ_2. This stress state is consistent with the background regional tectonic stress. However, when focal mechanisms were clustered into spatial and temporal groups, multiple stress states arise, with some varying significantly from the stress state when all the events were inverted. The deviation between inverted stress states from clustered events and inverted stress states using all the events may suggest that spatial and temporal stress heterogeneities exist within the reservoir. The deviations between inverted stress states of the clustered events and inverted stress states of all the events could be an artefact of the fact that some of the clusters have a very small number of events used for the stress inversions. This can increase the uncertainty of the inverted stress state. Therefore, there may not be enough focal mechanism data within each cluster to be confident that the inverted stress state is actually representative of the reservoir stress state.

The outcomes of the stress inversions identifies which of the two focal mechanism nodal planes was most likely to have slipped. Figure 12 shows one stereonet with the poles to all nodal planes and another stereonet with the poles to all the inferred slip planes after inverting all the focal mechanisms. The four colored crosses indicate the poles to the model fault surfaces nearest the microseismic events. The inferred slip planes appear to be subparallel with the model fault surfaces, with some variation. This may suggest that slip in the reservoir is occurring on or near the faults.

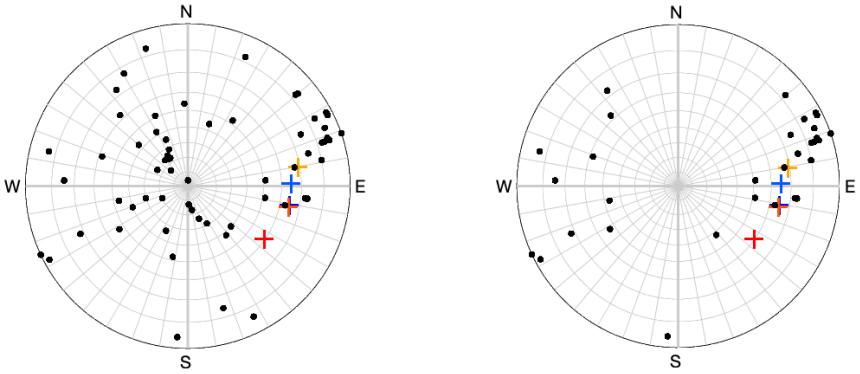

Figure 12: Poles to focal mechanism nodal planes (left) and poles to inferred slip planes (right) from stress inversion using all events indicated by black circles. Colored crosses indicate poles to model fault surfaces.

Using the reservoir normal/strike-slip stress model, it is possible to check if the heterogeneities of clustered inverted stress orientations are consistent with modeled stress orientations. To do this, the principal stress directions are calculated from the modeled stress tensors at the locations of the microseismic events. We assumed four model constraints for the initial stress conditions generated by the GEOSX model: (1) and $S_{H,\,max}$ azimuth of N20E, (2) a normal/strike-slip faulting environment, such that the magnitudes of SHmax and SV are equal, (3) a critically stressed environment, and (4) a frictional coefficient of 0.6 (Byerlee, 1978) for all reservoir rocks.

Since the stress model does not currently consider stress changes through time, only compare the modeled and inverted stress states of the spatial clusters can be compared. The model derived principal stress directions are plotted with the focal mechanism inverted principal stress directions for the five spatial clusters in Figure 13.

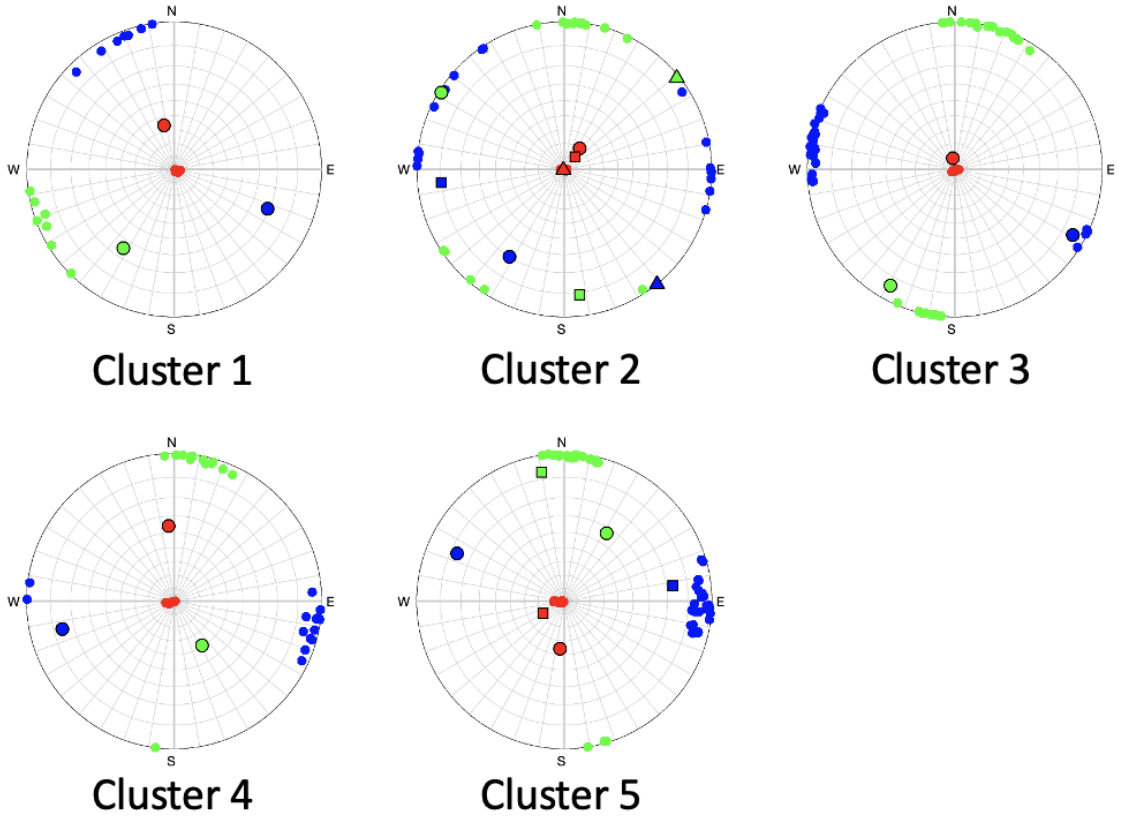

Figure 13: The model derived principal stress directions plotted with the focal mechanism inverted principal stress directions for the five spatial clusters. The red, green, and blue markers correspond to the inverted directions of σ_1, σ_2, and σ_3, respectively. Markers without black outlines indicate modeled stress directions at locations of microseismic events. Markers with black outlines indicate inverted stress directions from focal mechanism solutions. Markers of similar shape correspond to unique inverted stress states.

In S1, the modeled σ_2 orientation appears to be oriented horizontally in a Northeast/Southwest direction, whereas in S2 through S5, the modeled σ_2 orientation appears to be oriented horizontally in a North/South direction, consistent with the inferred regional stress. The inverted stress states from S1 and S5 are generally consistent with their respective model stress states, barring the fact that the inverted stress orientations are slightly offset from being vertical and horizontal. Two of the three inverted stress states from S2 are consistent with the respective modeled stress states. The inverted stress states from S3 are consistent with the respective modeled stress states. There is an inconsistency between the modeled and inverted stress state in S4. The inverted stress state of S4 does not suggest any principal stress near vertical. S1 is the furthest cluster from the injection and production wells, whereas S 2 through S5 are nearest to the two northernmost production wells. This slight rotation of modeled σ_2 orientation may be indicating a spatial shift in reservoir stress orientation to the west of the northernmost production wells.

Although some of the inverted and modeled stress states appear to show some general agreement, there are still discrepancies between the two. One of the discrepancies may be due to the fact that the model currently does not capture changes in stress due to fluid and heat production. Therefore, any additional stress heterogeneities that may have developed due to production and associated fault slip within the reservoir is not captured by the model. Additionally, the lack of recovered focal mechanisms are a cause of uncertainty of the inverted stress states. A larger sample size of focal mechanisms would better constrain the inverted stress state, potentially providing less uncertainty in the inverted stress states. The magnitude of the stress changes caused by production also needs to be evaluated.

6. CONCLUSIONS

The purpose of this study was to aid in constraining the initial stress condition to be used in the reservoir-scale GEOSX hydro-thermo-mechanical model as part of the WHOLESCALE project, which attempts to understand the spatial and temporal evolution of stress in a geothermal reservoir in San Emidio, Nevada, United States. This study used focal mechanism solutions recovered from microseismic events that were the result of a shut-in that occurred in 2016. Linear stress inversions were performed on the focal mechanism solutions in order to constrain the reservoir stress. Stress heterogeneity within the reservoir was further investigated by performing stress inversions on focal mechanisms that were clustered into spatial and temporal groups. Results from the stress inversions indicated that when viewing the reservoir stress state as a whole, the reservoir stress is consistent with the background regional tectonic stress. However, within the spatial and temporal clusters, the inverted stress states deviate from the background regional tectonic stress, possibly indicating smaller-

scale stress heterogeneities within the reservoir. There is some agreement between the inverted and modeled stress states when SHmax= SV, and an SHmax azimuth consistent with background regional tectonic stress.

Further work must be done in order to constrain the initial stress distribution that will be most representative of the reservoir stress. Additional focal mechanisms should be recovered from microseismic events which are expected to occur form a shut-in scheduled to occur in early 2022. A similar analysis of the focal mechanisms in this study can be applied to the recovered focal mechanisms that will be obtained in 2022. The analysis of the future focal mechanism data will lead to updated insights as to how the reservoir stresses have evolved in both space and time since 2016.

ACKNOWLEDGEMENTS

We thank the following individuals for skillful assistance in the field: Joe Pavone, Clifford Reed, Alan Pinuelas, Zack Young, Quaid Ricks, and Chris Gates.

We thank Bill Barker and Charlie Stevens at Microseismic Inc. for helpfully providing information regarding the seismic survey in December 2016.

We gratefully acknowledge support from the Weeks family to the Department of Geoscience at the University of Wisconsin-Madison.

We acknowledge image data acquired by the TerraSAR-X (Pitz and Miller, 2010) and TanDEM-X (Krieger *et al.*, 2007) satellite missions operated by the German Space Agency (DLR). These data were used under the terms and conditions of Research Project RES1236. Image data were also acquired by the SENTINEL-1 satellite mission (Salvi *et al.*, 2012) operated by the European Space Agency (ESA).

The work presented herein has been funded in part by the Office of Energy Efficiency and Renewable Energy (EERE), U.S. Department of Energy, under Award Numbers DE-EE0007698 and DE-EE0009032.

REFERENCES

Byerlee, J. "Friction of rocks." *Rock friction and earthquake prediction*. Birkhäuser, Basel, 1978. 615-626.

Folsom, M., Libbey, R., Feucht, D., Warren, I., Garanzini, S., 2020. Geophysical Observations and Integrated Conceptual Models of the San Emidio Geothermal Field, Nevada. In 45th Proceedings of Workshop on Geothermal Reservoir Engineering, Stanford University, Stanford, California, 10-12 February 2020.

Heidbach, O., M. Rajabi, X. Cui, K. Fuchs, B. Müller, J. Reinecker, K. Reiter, M. Tingay, F. Wenzel, F. Xie, M. O. Ziegler, M.-L. Zoback, and M. D. Zoback (2018): The World Stress Map database release 2016: Crustal stress pattern across scales. Tectonophysics, 744, 484-498, doi:10.1016/j.tecto.2018.07.007

Hickman, S. H. and N. C. Davatzes (2010) In-situ stress and fracture characterization for planning of an egs stimulation in the Desert Peak geothermal field, Nevada. USGS Staff -- Published Research. 418.

Hickman, S., Zoback, M., & Benoit, R. (1998). Tectonic controls on reservoir permeability in the Dixie Valley, Nevada , geothermal field.

Kreemer, C., Blewitt, G., and Klein, E. C. (2014), A geodetic plate motion and Global Strain Rate Model, *Geochem. Geophys. Geosyst.*, 15, 3849– 3889, doi:10.1002/2014GC005407.

Matlick, S., (1995). San Emidio Geothermal System, Empire, NV. GRC Field Trip – October 1995. Mesquite Group, Inc

Michael, A. J. (1984). Determination of stress from slip data: faults and folds, J. Geophys. Res. 89, 11,517–11,526.

Alan Morris, David A. Ferrill, D.Brent Henderson; Slip-tendency analysis and fault reactivation. *Geology* 1996;; 24 (3): 275–278. doi: https://doi.org/10.1130/0091-7613(1996)024<0275:STAAFR>2.3.CO;2

Siler, D.L., Faulds, J.E., Mayhew, B., and Mcnamara, D.D., 2016, Geothermics Analysis of the favorability for geothermal fluid flow in 3D: Astor Pass geothermal prospect, Great Basin, northwestern Nevada, USA: Geothermics, v. 60, p. 1–12, doi: 10.1016/j.geothermics.2015.11.002.

Vavrycuk, V. (2014). Iterative joint inversion for stress and fault orientations from focal mechanisms. Geophysical Journal International. 199. 69-77. 10.1093/gji/ggu224.